

Development and computational fluid dynamics (CFD) simulation of cryostat thermal shielding for portable high purity germanium (HPGe) gamma spectrometer

Vladislav Malgin¹, Alan H. Tkaczyk^{2,3,*}, Oleg Yakovlev¹, Marti Jeltsov², Priit Priimagi²

¹ – Baltic Scientific Instruments (BSI), Ramulu street 3, LV-1005, Riga, Latvia;

² – Estflow Consulting OÜ, Narva maantee 9, EE-51013, Tartu, Estonia;

³ – University of Tartu, Institute of Technology, Nooruse 1, EE-50411, Tartu, Estonia.

* Corresponding author: Alan H. Tkaczyk, University of Tartu, Institute of Technology, Nooruse 1, EE-50411, Tartu, Estonia, tel. +372 7376523, e-mail: alan@ut.ee

Abstract

The effect of vacuum degradation in cryostat of a gamma spectrometer on the steady-state temperature of thermal shield and its efficiency are analyzed in this study. Considering the thermal load due to radiation, the thermal conductivity of residual gases and shield supports, the steady-state temperature of the shield is determined based on the differential energy balance equation for a simplified thermal model of the cryostat. A more complex model corresponding to the design of a real cryostat is simulated using computational fluid dynamics (CFD) in the Star-CCM+ environment. The obtained temperature distribution is presented. The simulated results are compared with experimental data measured on an operating cryostat with cryocooler Thales LSF4589 in the temperature stabilization mode. The same measurements were carried out for a cryostat with and without a thermal shield, as well as multilayer insulation. The obtained results confirm that the thermal shield provides heat transfer decreasing even for a vacuum degradation in a cryostat.

Keywords: Thermal shield; portable gamma spectrometer; high purity germanium (HPGe); computational fluid dynamics.

Nomenclature

A - cross-sectional area of thermal shield, m^2 ;

b - thermal shield shell thickness, m ;

K_n – Knudsen number;

k - thermal conductivity, $W / m \cdot K$;

L – length of the thermal shield, m ;

p - gas pressure, Pa ;

$Q_{i,j}$ - heat transfer between i - and j -surfaces, W ;

R - universal gas constant equals $8.3145 \text{ J} / \text{mol} \cdot \text{K}$;

S_i - area of i -surface involved in heat transfer, m^2 ;

T_i - temperature of i -surface, K ;

α_i - coefficient of accommodation for i -surface involved in heat transfer;

γ - adiabatic index for residual gas;

ε_i - coefficient of emissivity for i -surface involved in heat transfer;

λ - mean free path of molecules, m ;

μ - molar mass of the residual gas, kg / mol ;

σ - Stefan-Boltzmann constant equals $5.67 \cdot 10^{-8} W / m^2 \cdot K^4$;

Introduction

The current situation in the commercial market of small-sized and sufficiently reliable Stirling cryocoolers has made it possible to develop a wide range of gamma-spectrometric equipment based on high purity germanium (HPGe) detectors. The application of HPGe detectors as sensors assumes their cooling to cryogenic temperatures. Cooling through electromechanical Stirling cryocoolers has significant advantages over liquid nitrogen cooling, especially for portable devices intended for field applications, mobile radiation monitoring systems etc. [1-4].

However, the relative Carnot efficiency of commercially available Stirling cryocoolers does not exceed 7–12%, while for cryocoolers with pulse tube, it is even less. Therefore, reducing the heat transfer into the cryostat not only allows the use of cryocoolers with lower cooling capacity, which are more compact and lightweight but also significantly reduces the required battery capacity and its size. It is known that the heat transfer in a vacuum chamber is carried out due to the thermal conductivity of structural materials, the molecular conductivity of residual gases and thermal radiation [5-9].

Typically, in the operating mode of the spectrometer when the cryostat is cooled, the zeolite sorption pump maintains a high vacuum with a level 10^{-6} - 10^{-7} mbar. In this case, the heat transfer by the conductance of residual gases is negligible and heat transfer by thermal radiation is dominant. The long periods of storage in the OFF-state with warmed cryostat are characteristic for portable spectrometers. In a warmed state, the sorption pump releases adsorbed gases, which leads to vacuum degradation in the cryostat. In this case, heat transfer by residual gases becomes dominant and subsequent cooling by a cryocooler with lower cooling power becomes impossible. Moreover, due to gas leakage through the

seals, the vacuum in the cryostat always tends to degrade with time. Extending the operational life between services is important for the practical use of portable spectrometers.

An effective method to reduce heat transfer in a cryostat due to thermal radiation is the application of thermal shields [5-9]. Hitherto, the efficiency of the thermal shielding is considered exclusively under high vacuum conditions [10-13], but aspects of its practical application in vacuum degradation are not analyzed in the scientific literature of open access.

In this study, the influence of vacuum degradation on the efficiency of thermal shielding is investigated. The calculations based on a differential equation for a simplified thermal model as well as 3D simulation and experimental verification were performed for the cryostat of portable gamma spectrometer HandSPEC produced by Baltic Scientific Instruments (BSI) company, Fig. 1.

First of all, the differential equation for the temperature of a thermal shield based on the energy balance is supplemented by the terms of the heat transfer due to the conductivity of residual gases. Solutions for various gas pressures in a cryostat are analyzed. Further, the temperature distribution in a 3D-model of the cryostat with a thermal shield based on computational fluid dynamics (CFD) simulation is obtained. Finally, the results of calculations were confirmed by experimental investigations of a cryostat with thermal shield.

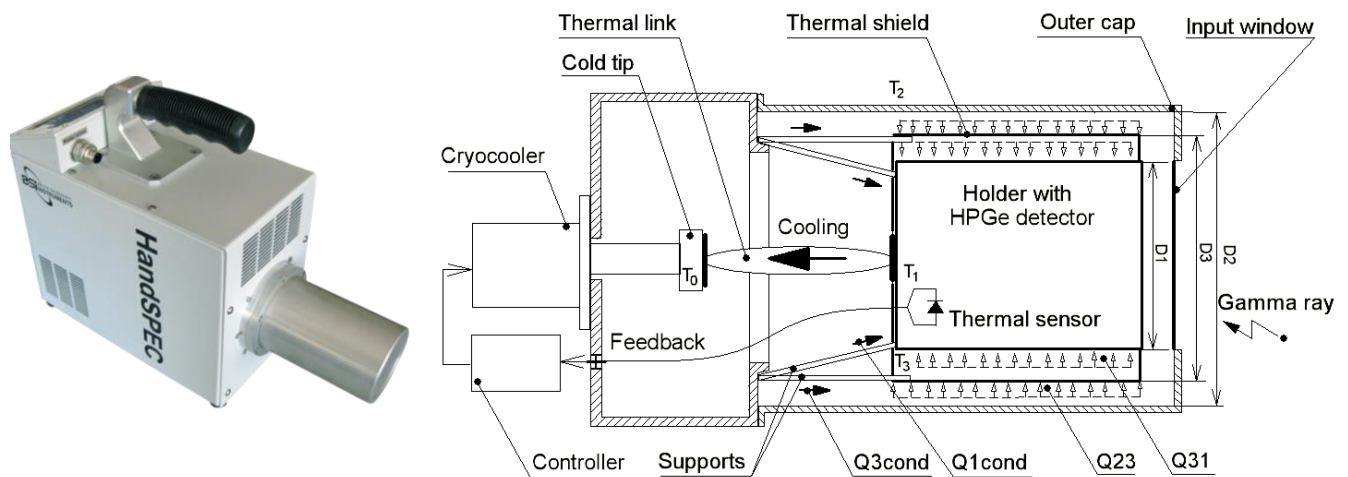


Fig. 1 Portable gamma spectrometer HandSPEC and heat flow in a cryostat with a thermal shield.

The simplified analytical model of a cryostat with a thermal shield

The steady-state temperature of thermal shield

The total heat transfer in vacuum chambers is a sum of the heat conduction through supports; residual gas conduction; thermal radiation and is described in detail in [5-9]. The calculations of steady-state temperatures of thermal shield presented below are based on the energy balance equation for the incoming

heat flows and outgoing from it:

$$Q_{23} + Q_{3cond} = Q_{31}, \quad \text{where } Q_{23} = Q_{23rad} + Q_{23resid}, \quad Q_{31} = Q_{31rad} + Q_{31resid} \quad (1)$$

Based on the structure of cryostat with thermal shield, Fig. 1, the physical model for heat flows investigation can be represented in a form of coaxial cylinders with diameters D_1 , D_2 and D_3 , Fig. 2, a. The temperature in the circular direction considered to be unchanged and independent of supports location.

The heat transfer due to thermal radiation and gas conductance are described by well-known equations:

$$Q_{i,jrad} = \varepsilon_{i,j} \cdot \sigma \cdot S_j \cdot (T_i^4 - T_j^4), \quad \text{where: } \varepsilon_{i,j} = 1 / \left(\frac{1}{\varepsilon_i} + \left(\frac{1}{\varepsilon_j} - 1 \right) \cdot \frac{S_i}{S_j} \right), \quad (2)$$

$$Q_{i,jresid} = \alpha_{i,j} \cdot B \cdot S_j \cdot p \cdot (T_i - T_j), \quad \text{where: } \alpha_{i,j} = 1 / \left(\frac{1}{\alpha_i} + \left(\frac{1}{\alpha_j} - 1 \right) \cdot \frac{S_i}{S_j} \right), \quad B = \frac{\gamma + 1}{\gamma - 1} \cdot \sqrt{\frac{R}{8\pi\mu \cdot T_2}}, \quad (3)$$

It is assumed that in the operating pressure range the mean free path of molecules is greater than the distance between surfaces in a cryostat under investigation. The heat transfer due to residual gas corresponds to the molecular regime conductivity, depends on pressure p . Typically, the distances between the vacuum cap, thermal shield and detector holder, are much smaller than their length. This allows to use for ε_i and α_i analytical formulas for infinite coaxial cylinders.

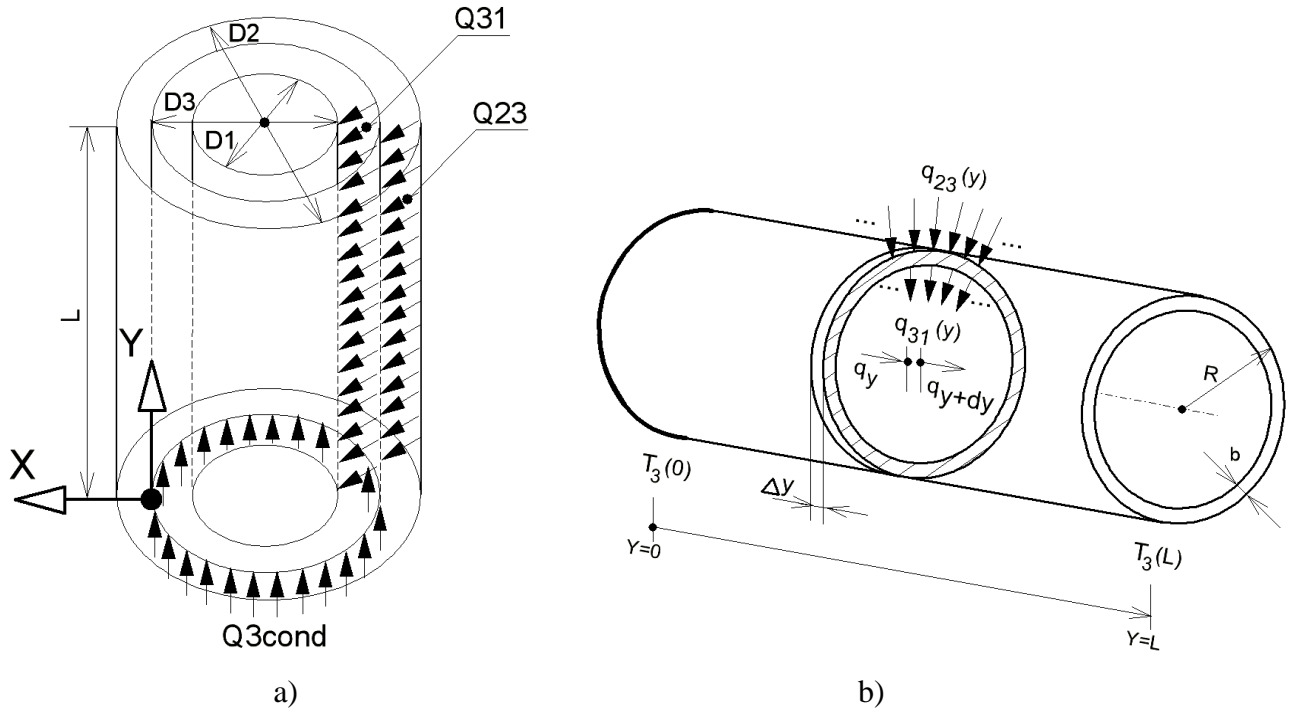


Fig. 2 Simplified models of the cryostat and the thermal shield with heat deposition $q(y)$

The energy balance applied to element Δy when heat transferred along axe Y , leads to the equation:

$$q_y + \Delta q_c = q_{y+\Delta y}, \quad \text{where } \Delta q_c = \Delta q_{23rad} - \Delta q_{31rad} + \Delta q_{23resid} - \Delta q_{31resid}. \quad (4)$$

When the equation (4) is divided by Δy and the limit is taken as $\Delta y \rightarrow 0$, after substituting the Fourier's law, a second-order differential equation with constant coefficients is obtained.

$$k \cdot A \cdot \frac{d^2 T}{dy^2} - \frac{dq_c}{dy} = 0, \quad \text{where } A = b \cdot \pi \cdot D_3 \cdot \left(1 - \frac{b}{D_3}\right) \quad \text{and} \quad (5)$$

$$dq_c = \varepsilon_{23} \sigma \cdot dS_3 \cdot (T_2^4 - T^4) - \varepsilon_{31} \sigma \cdot dS_1 \cdot (T^4 - T_1^4) + \alpha_{23} Bp \cdot dS_3 \cdot (T_2 - T) - \alpha_{31} Bp \cdot dS_1 \cdot (T - T_1). \quad (6)$$

$$\text{Since:} \quad \frac{dS_3}{dy} = \pi \cdot D_3, \quad \frac{dS_1}{dy} = \pi \cdot D_1, \quad (7)$$

the differential equation (5) which describes the steady-state temperature distribution on thermal shield due to thermal radiation and molecular conductivity of residual gases can be rewritten as:

$$k \cdot b \cdot \left(1 - \frac{b}{D_3}\right) \frac{d^2 T}{dy^2} = \sigma \cdot [\varepsilon_{23} (T_2^4 - T^4) + \varepsilon_{31} \frac{D_1}{D_3} (T^4 - T_1^4)] + B \cdot p \cdot [\alpha_{23} \cdot (T - T_2) + \alpha_{31} \frac{D_1}{D_3} \cdot (T - T_1)]. \quad (8)$$

The boundary conditions set the initial temperature at the beginning of the shield $T_3(0)$ and simulate stop of further heat transfer at the end of the thermal shield:

$$T_{y=0} = T_3(0) \quad \text{and} \quad \frac{dT_{y=L}}{dy} = 0. \quad (9)$$

Equation (8) was solved numerically for the parameters corresponding to the cryostat of the spectrometer HandSPEC and indicated below: $D_1 = 50 \text{ mm}$, $D_2 = 80 \text{ mm}$, $D_3 = 72 \text{ mm}$. The temperatures of the detector and vacuum cap assumed constant $T_1 = 90 \text{ K}$ and $T_2 = 295 \text{ K}$.

The emissivity and accommodation coefficients presented in references ^[5-9] differ greatly depending on impurities, oxidation and surface processing. This indeterminacy reduces the importance of accuracy calculation in comparison with the observed trends. In cryostat, the outer cap is made from mechanically treated aluminum: $\varepsilon_2 = 0.2$, $\alpha_2 = 0.9$. For aluminum detector holder is assumed $\varepsilon_1 = 0.3$, $\alpha_1 = 1.0$.

Typically, thermal shields are made from aluminum or copper ^[10-13]. In cryostat under investigation, the shield is very short ($L = 0.1 \text{ m}$), it is allowed to make it of electropolished stainless steel with a thickness $b = 0,5 \text{ mm}$ which is more technological ^[14]. For this case: $k = 17 \text{ W/m} \cdot \text{K}$, $\varepsilon_3 = 0.1$, $\alpha_3 = 0.9$.

The residual gases in the vacuum chamber of cryostat are formed due to leakage through the seals and by outgassing. Therefore, its composition is close to air, so $\gamma = 1.41$ and $\mu = 0.029 \text{ kg/mol}$.

As an example, the steady-state temperature distribution of the thermal shield along the y -axis for variable initial temperatures $T_3(0)$ and residual gases pressures p presented in Fig. 3. Note, that heat transfer due to radiation and molecular conductivity of residual gases is distributed uniformly over the area of the thermal shield. Therefore steady-state temperature for “floating” shield ($Q_{3cond} = 0$) can be obtained by equating the right-hand side of (8) to zero. The temperatures for “floating” thermal shield are calculated and presented in Fig. 3 by a black dashed line.

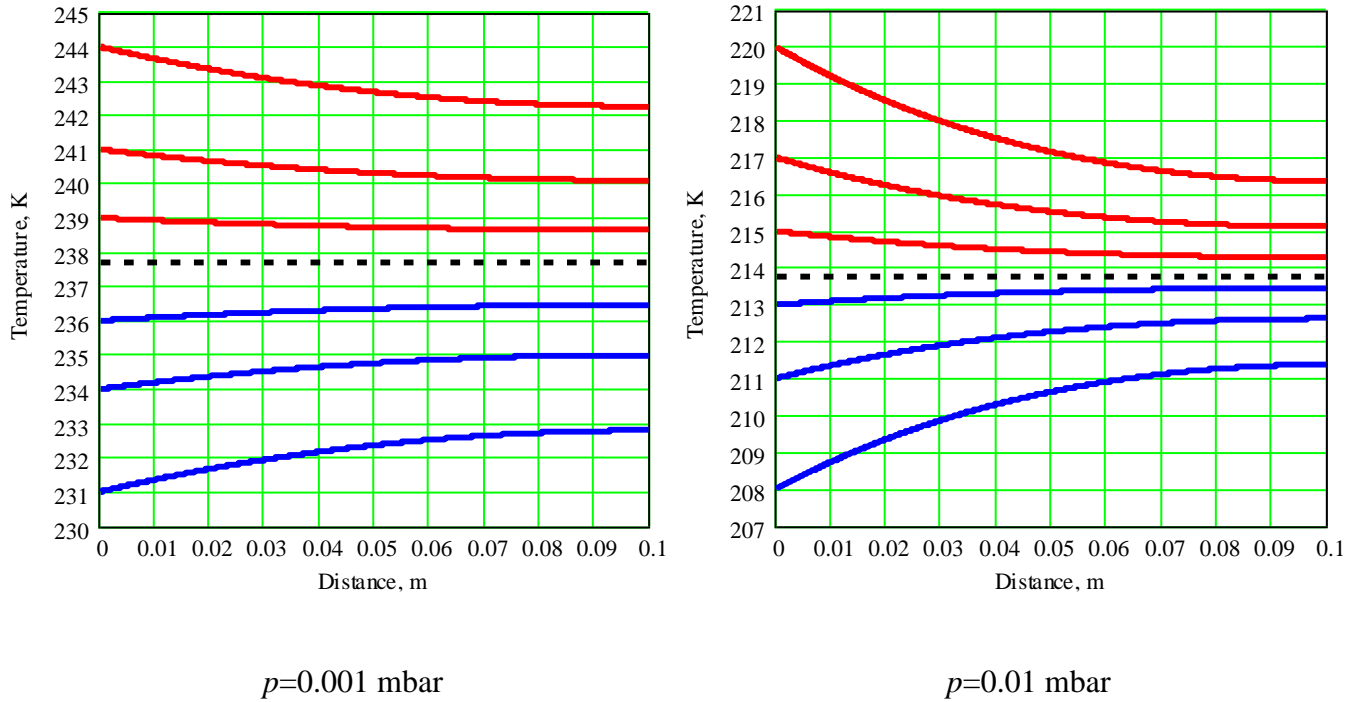


Fig. 3 Solutions of the differential equation (8) for variable initial temperatures $T_3(0)$

The uneven temperature on the shield surface with the difference between ends ΔT is provided by heat inflow Q_{3cond} through supports. Red curves represent the temperature distribution for positive heat inflow through supports whereas the blue curves - for negative heat inflow provided by active cooling. The active cooling decreases the temperature of thermal shield but complicates the design of cryostat [15-17]. For initial temperatures $T_3(0)$ used in Fig. 3 the values of Q_{3cond} was estimated by numerical integration of equation (6) at Y -axis, and presented in Table 1. The obtained values of Q_{3cond} make it possible to estimate the required thermal resistance of the shield supports R_{3th} based on the desired heat inflow Q_{3cond} :

$$R_{3th} = [T_2 - T_3(0)] / Q_{3cond} \cdot \quad (10)$$

With increasing heat inflow through supports Q_{3cond} the temperature difference ΔT increases also. Analysis of the temperature distribution allows to estimate the allowable metal thickness for thermal shield manufacture. In the present case, the surface is quasi-isothermal and application of 0.5 mm stainless steel is sufficient, although its thermal conductivity is worse than that of aluminum or copper.

Table 1. The necessary heat inflow through the supports Q_{3cond} providing the specified initial temperatures $T_3(0)$ and the resulting temperature difference ΔT between ends of the thermal shield

Type of shield	Pressure, p=0.001 mbar			Pressure, p=0.01 mbar		
	$T_3(0)$	ΔT	Q_{3cond}	$T_3(0)$	ΔT	Q_{3cond}
shield with positive heat inflow	244 K	1.74 K	0.072 W	220 K	3.64 K	0.165 W
	241 K	0.90 K	0.037 W	217 K	1.88 K	0.085 W
	239 K	0.35 K	0.014 W	215 K	0.71 K	0.032 W
“floating” shield with zero heat inflow	237.71 K	0	0	213.78 K	0	0
shield with negative heat inflow	236 K	-0.46 K	-0.019 W	213 K	-0.46 K	-0.021 W
	234 K	-1.00K	-0.041 W	211 K	-1.62 K	-0.076 W
	231 K	-1.79K	-0.074 W	208 K	-3.37 K	-0.153 W

Table 2. The balance between the coming and outgoing heat transfers of the thermal shield for varied pressure in the cryostat. The components due to thermal radiation Q_{23rad} , Q_{31rad} ; conductivities of residual gases $Q_{23resid}$, $Q_{31resid}$ and supports Q_{3cond} are indicated.

Pressure in a cryostat	Calculated temperature of shield, T_3	Total heat transfer Q_{23} and its components coming to thermal shield from outer cap				Total heat transfer Q_{31} and its components outgoing from thermal shield to detector		
		Q_{3cond}	Q_{23rad}	$Q_{23resid}$	Q_{23}	Q_{31rad}	$Q_{31resid}$	Q_{31}
0.0001 mbar	252.32 K	0.053 W	0.332 W	0.009 W	0.394 W	0.367 W	0.027 W	0.394 W
0.001 mbar	242.36 K	0.066 W	0.389 W	0.114 W	0.569 W	0.312 W	0.257 W	0.569 W
0.01 mbar	215.94 K	0.099 W	0.509 W	1.707 W	2.315 W	0.194 W	2.121 W	2.315 W
0.02 mbar	211.09 K	0.105 W	0.527 W	3.623 W	4.255 W	0.177 W	4.078 W	4.255 W

The estimation of heat transfer components

The components of heat transfer for a thermal shield calculated according to the energy balance equation (1) for various residual gas pressures are presented in Table 2. The thermal shield has been mounted on the three bars 5x5x15 mm made from polyimide. The total thermal resistance equals $R_{th} = 800 \text{ K/W}$, to provide the heat inflow $Q_{3cond} \leq 0.1 \text{ W}$ in operating temperatures range. It is observed that, for a high vacuum (pressure is less than 10^{-3} mbar); the heat transfer due to thermal radiation is dominant. On the contrary, for the case of a vacuum degradation, the heat transfers due to molecular conductivity of residual gases became dominant and the steady-state temperature of thermal shield decreases.

Comparison of the heat transfer to the detector in a cryostat with and without a thermal shield is presented in Table 3. In a cryostat without thermal shield, the heat transfer to detector due to thermal radiation Q_{21rad} remains constant. But in cryostat with thermal shield, the heat transfer Q_{31rad} decreases when pressure increases. This unexpected at first glance difference is explained by a decrease of the thermal shield's temperature with increasing pressure due to the molecular conductivity of residual gases (please see Tables 1,2). The results obtained indicate that the efficiency of thermal shielding estimated by ratio Q_{21} / Q_{31} is preserved even in the case of a vacuum degradation in a cryostat.

The temperature distribution in the 3D model of the cryostat

It should be noted that the results obtained in the previous section are based on a model of a cryostat with a thermal shield as coaxial cylinders, Fig. 2. This simple model allows us to understand and evaluate the main heat fluxes between the outer cap, thermal shield and HPGe detector. But such parts of the cryostat as supports, thermal link, cassette with zeolite, etc., fall out of the investigations presented in the previous section due to their more complex geometry.

A three-dimensional CFD model of the cryostat was created to carry out detailed steady-state temperature distribution and the heat transfer within the device. Technical drawings of the cryostat as CAD files from SolidWorks environment were imported to a commercial CFD software package Star-CCM+ (version 13.02) [18] which was used for geometry pre-processing, meshing, physics modeling, simulation and for post-processing of the results. Once calibrated, the model becomes a valuable tool for in-depth analysis and optimization of the final design of a cryostat.

Table 3. The comparison of heat transfers coming to the detector at various residual gas pressures for a cryostat with and without a thermal shield. The components due to thermal radiation Q_{31rad} , Q_{21rad} and conductivity of residual gases $Q_{31resid}$ and $Q_{21resid}$ are indicated.

Pressure in a cryostat	Total heat transfer Q_{31} and its components to detector from thermal shield			Total heat transfer Q_{21} and its components to detector from outer cap (without thermal shield)			Ratio Q_{21} / Q_{31}
	Q_{31rad}	$Q_{31resid}$	Q_{31}	Q_{21rad}	$Q_{21resid}$	Q_{21}	
0.0001 mbar	0.367 W	0.027 W	0.394 W	1.146 W	0.035 W	1.181 W	2.99
0.001 mbar	0.312 W	0.257 W	0.569 W	1.146 W	0.348 W	1.494 W	2.63
0.01 mbar	0.194 W	2.121 W	2.315 W	1.146 W	3.481 W	4.627 W	2.00
0.02 mbar	0.177 W	4.078 W	4.255 W	1.146 W	6.961 W	8.107 W	1.91

The surface-to-surface radiation model is used to analyze the thermal heat transfer between the surfaces of arbitrary complexity, that form enclosed space inside the spectrometer. The residual gas conduction model is based on the temperature jump model at the solid-vacuum interface [19]. Conduction heat transfer through solids (and in a rarefied gas environment) is modeled using segregated energy model. This allows to calculate the temperature distributions in different parts with different materials in the spectrometer, such as aluminum, stainless steel, copper, polyimide.

An external and cross-section views of the full cryostat CAD model are shown in Fig. 4. The CFD model includes all internal parts of the cryostat except electric leads and hardware. A common temperature field observed in the simulations is shown in Fig. 5. Cryostat housing is at environment temperature. The largest thermal gradient is accommodated in the supports' rings between the housing and internal components which are at the lowest temperature as they are connected to the cryocooler. While not shown in detail here, the model allows to study the heat balance for every device component. All results presented hereon are converged in terms of residuals as well as integral heat balance.

Temperature distribution on the surface of the thermal shield calculated by the CFD model is presented in Fig. 6, a. The analysis was made for vacuum conductivity level $0.005 W / m \cdot K$. In the lower part of the shield, the attachment points of the supports stand out. The temperature distribution calculated in the framework of the previous model based on coaxial cylinders is shown in Fig. 6, b. It can be seen that the axial temperature distribution calculated by two different methods are close to each other as well as to the experimental data presented below. The remaining discrepancy of the calculation results (less than 1 K) is

acceptable and can be attributed to the uncertainties in the model as well as in the physical measurements. It should be emphasized that steady-state axial temperature drops along the length of the thermal shield in both cases about 1.1 K. Slight temperature difference between the beginning and end of the thermal shield can be explained by the small heat inflow through the supports.

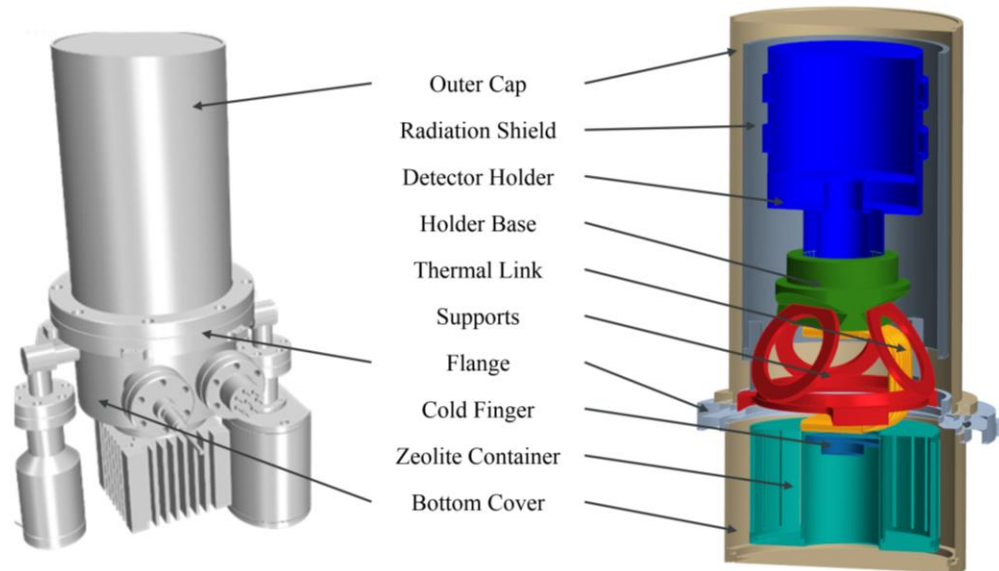


Fig. 4 An external and cross-section views of the cryostat CAD model in the CFD software.

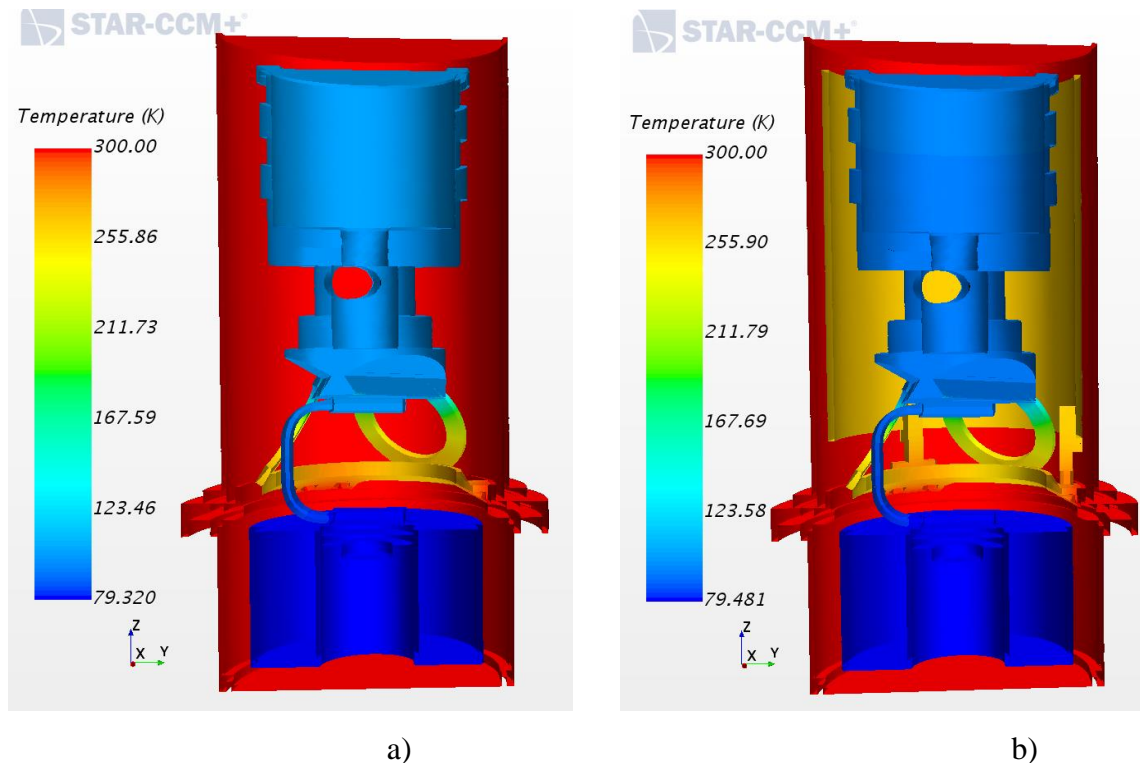


Fig. 5 Temperature distribution on internal parts of cryostat: (a) without thermal shield; (b) with thermal shield.

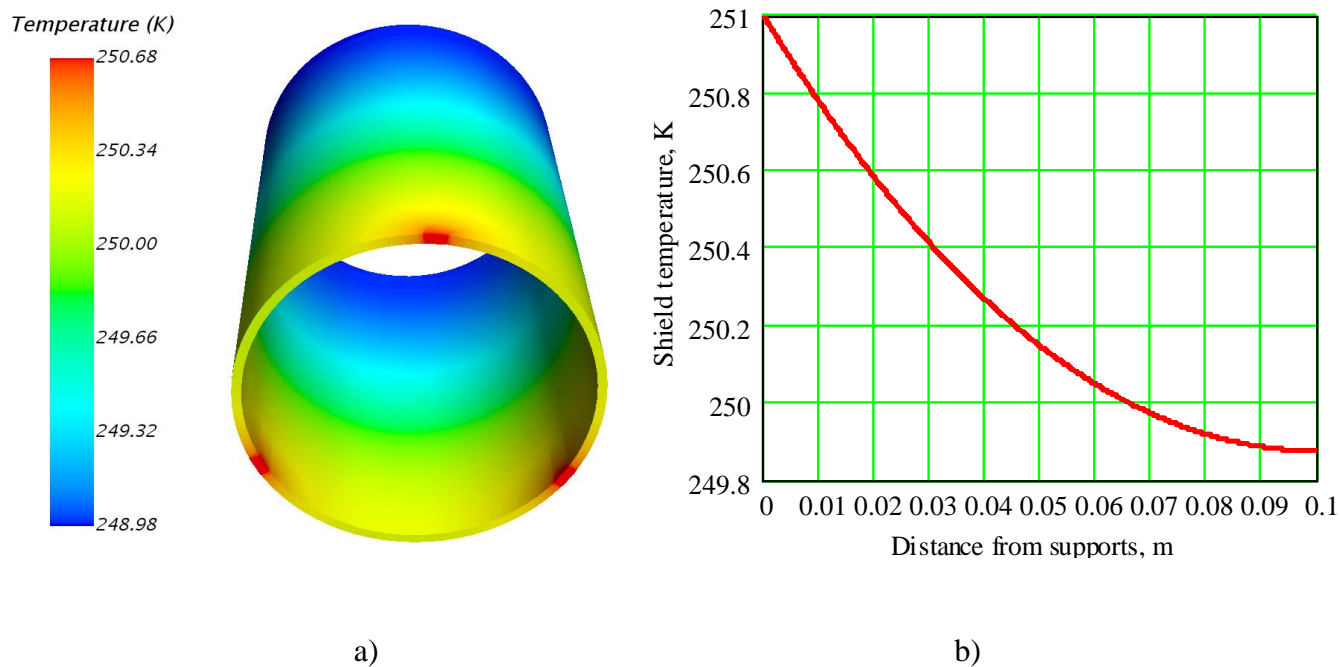


Fig. 6 Local steady-state temperature distribution on the surface of thermal shield calculated by:
 (a) CFD model; (b) differential equation (8) for $p=2.0 \times 10^{-4}$ mbar.

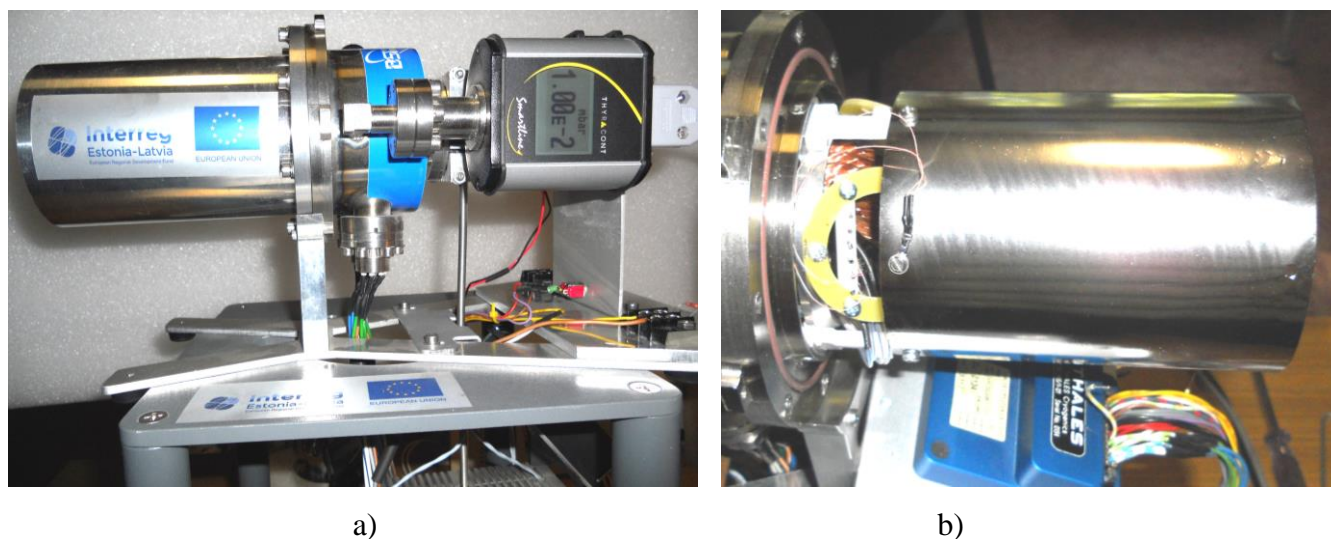


Fig. 7 The test cryostat (a) its appearance; (b) thermal shield with a PT100 sensor

Experimental results

The cryostat of a portable spectrometer prepared for experimental investigations was equipped with pressure gauge Thyracont VSP64DL and additional temperature sensors PT100 to measure the temperatures of the cryocooler's cold tip, HPGe detector and thermal shield, Fig. 7. Before measurements, the baked cryostat was subjected to long-term pumping out to reduce outgassing from internal surfaces. The Thales LSF 9589 cryocooler provides cooling power 2.7 W at 80 K for input power 80 W.

During experiments, the temperature stabilization mode of the detector with $T_1 = 90\text{ K}$ was implemented. The measured temperatures on control points for varied pressures in cryostat are presented in Fig. 8. The obtained results show that the cryocooler provides stabilization of detector temperature while the pressure is less than 6.2×10^{-3} mbar. At the same time, the temperature of the thermal shield decreases from 254 K to 228 K, and the input power of the cryocooler increases from 34 W to 77 W. Reducing the steady-state temperature of the thermal shield provided by energy balance can be explained by an increase in heat transfer due to the molecular conductivity of the residual gases.

With a further increase in pressure in the chamber, the cryocooler's cooling power is not enough to stabilize the temperature of the detector. The temperature of thermal shield increases due to increasing the temperature T_1 . The growth in heat transfer provided by a growth in the pressure of residual gases in a cryostat is confirmed by the proportional changes in the temperature difference $T_1 - T_0$ on the thermal link which has a constant thermal resistance.

The temperatures of the thermal shield calculated based on the differential energy balance equation (8) are marked by crosses and are closed to that measured experimentally, Fig. 7. For calculations, the measured temperature T_1 was used. Note that the physical model used assumes the molecular regime of heat transfer for residual gases. The boundaries between different regimes in the kinetic theory of gases are rather arbitrary. However, it is generally accepted that at $K_n = \lambda / d \geq 10$ only molecular regime exists. At lower K_n values, the transition (Knudsen) regime begins ^[20]. The characteristic distance for cryostat is about $d = (D_2 - D_3) / 2 = 4\text{ mm}$ and the pressure estimation for $K_n \geq 10$ is $p < 2.0 \times 10^{-4}$ mbar. Falling into the beginning of the transition regime explains some divergence of the curves with increasing gas pressure.

The same series of measurements were carried out for a cryostat without a thermal shield, as well as multilayer insulation has been used as a thermal shield. A multilayer insulation Coolcat 2 NW produced by Swiss technology group Ruag Space and composed of 10 layers of double-sided aluminized polyester foil was used. The results are presented in Fig. 9 together with the same dependence for a cryostat with a thermal shield shown in Fig. 8. The temperature stabilization mode stops at 2.1×10^{-3} mbar in the cryostat without a thermal shield and continues to a pressure of 6.2×10^{-3} mbar when it is installed. When multilayer insulation is used the temperature stabilization range is extended for 1.2×10^{-2} mbar. This extension of the range of stabilization of the temperature of the detector with limited cooling power confirms the retention of the efficiency of thermal shielding in the case of vacuum degradation. The data obtained from the experiments correspond to conclusions based on the calculated data given in Tables 2 and 3.

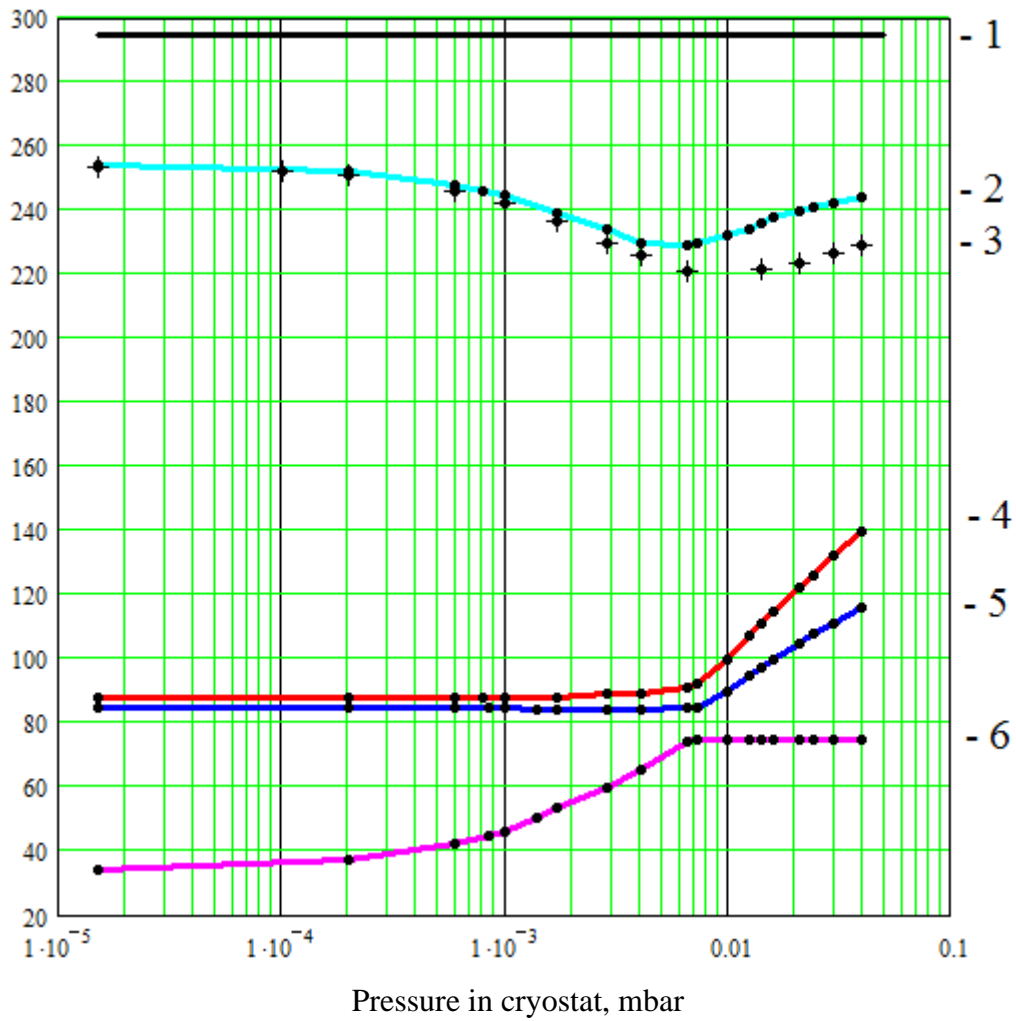


Fig. 8 The temperatures on control points and cryocooler's input power for varied pressures.

The curves are labeled as followed:

- 1 - Temperature of the outer cap (ambient temperature) T_2 , K;
- 2 – Temperature of thermal shield measured experimentally T_3 , K;
- 3 – Temperature of thermal shield calculated by the energy balance equation T_3 , K;
- 4 – Temperature of the detector T_1 , K;
- 5 – Temperature of cryocooler's "cold tip" T_0 , K;
- 6 – Input power of cryocooler P_{in} , W;

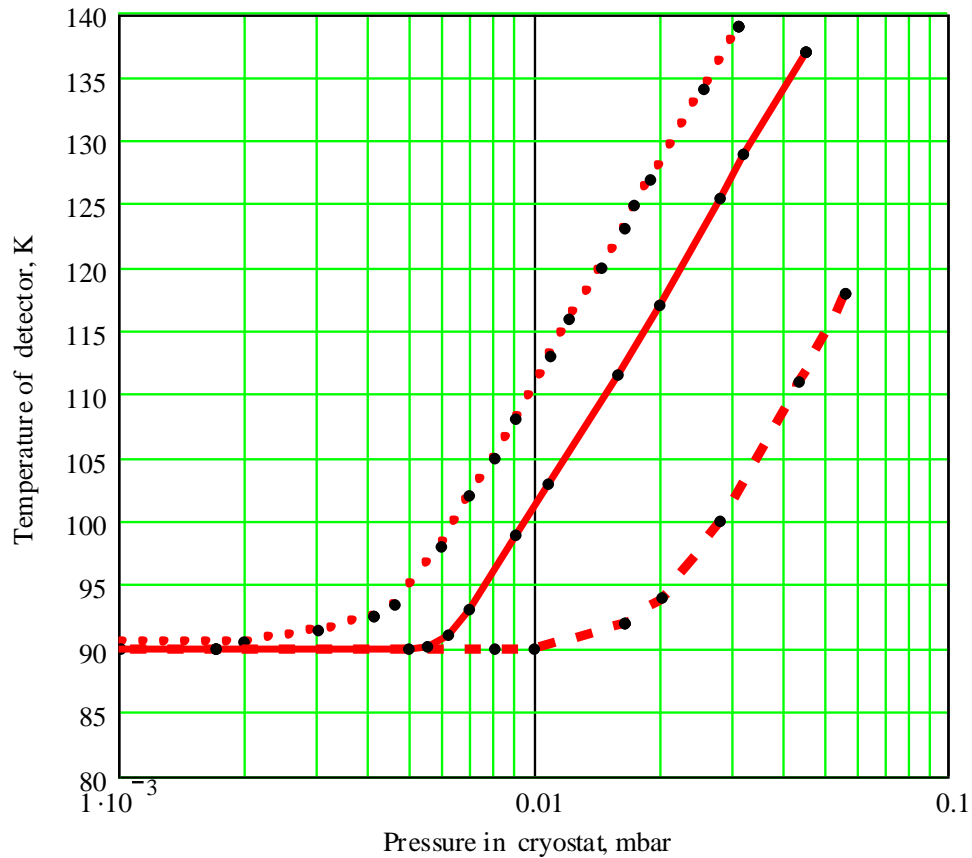


Fig. 9 The temperatures of the detector in a cryostat without thermal shield; with thermal shield; and with multilayer insulation (dotted, solid and dashed curves, respectively).

Note that from a physical point of view, each layer of multilayer insulation plays the role of a thermal shield ^[8-9]. This explains its high efficiency. However, an extremely large total surface area increases the outgassing greatly. So, increased risk of highly sensitive HPGe detectors contamination reduces its attractiveness in portable spectrometers intended for widespread use.

Results and discussion

The analysis results of heat flow in a cryostat with a thermal shield under vacuum degradation are presented. The differential equation for the temperature distribution of the thermal shield, based on the energy balance, is supplemented by terms that take into account heat transfer due to the molecular conductivity of the residual gases in the cryostat. The theoretical analysis was verified by experiments performed on a cryostat of a HandSPEC portable gamma-ray spectrometer. It was found that the thermal shield reduces the heat transfer to the detector not only due to radiation but also because of the molecular conductivity of the residual gases. The digital twin of a real cryostat in the Star-CCM + commercial

package was created and verified based on cross-comparison of results. The performed experiments confirmed that the presence of a thermal shield in cryostat increases the upper-pressure limit at which the detector can be cooled without increasing the cryocooler power.

Note that the presented effect of residual gas pressure on the temperature of the thermal shield can be used to control vacuum degradation during operation with a cooled cryostat. A monotonic decrease in the temperature of the thermal shield from 254 K to 228 K with a change in pressure by three orders of magnitude was observed, Fig. 8. Comparing the temperatures of the thermal shield and the cooled detector is a much simpler and cheaper way to estimate the pressure of the residual gases in the cryostat (after preliminary calibration, of course) than using additional pressure gauges with a cold cathode.

This article investigated the positive effect of the thermal shield on reducing heat transfer during vacuum degradation in a cryostat for steady-state conditions. The temperature of the already cooled detector was kept constant. However, for cryostats with cryocoolers, the most critical is the cooling process itself. During vacuum degradation, the limited power of cryocoolers is not always enough to cool the detector to operating mode. This is especially true for cryostats of portable equipment, the operation of which is characterized by more frequent shutdowns, leading to the warming of the HPGe detector during storage between measurements. The study of cooling a cryostat with a thermal shield by a low power cryocooler as a dynamic process is a necessary development of the presented article. Simulation of the cooling process is supposed to be performed based on the digital twin in the commercial package Star-CCM +.

Conclusions

It seems that the completed and upcoming studies will help to determine technical solutions for extending the service life between maintenance of portable spectrometers designed for field applications.

The results can be useful for experts in the field of cryogenic technology.

Acknowledgements

This work has been carried out within the project "Hand-held spectrometer design" supported by the cross-border cooperation programme Interreg V-A — Estonia–Latvia, co-funded by the European Regional Development Fund. The paper reflects the views of the authors, and the managing authority of the programme is not liable for how this information may be used.

REFERENCES

- [1] Katagiri, M.; Birumachi, A.; Sakasai, K.;Takahashi, K. Portable Gamma-ray Monitor Composed of a Compact Electrically Cooled Ge Detector and a Mini-MCA system, IEEE Transactions on Nuclear Science Symposium, 2003, 50(4), 1043-1047.
- [2] Keyser, R. M.; Hagenauer, R. C. Performance of a Portable, Electromechanically-cooled HPGe Detector for Site Characterization. Journal of Radioanalytical and Nuclear Chemistry, 2008, 277(1), 149–153.
- [3] Yocum, K. M.; Martin, G. N.; Colaresi, J. F.; and Miley, H.S. Improvement in Ge Detector Cooling. Proceedings of the 30th Monitoring Research Review: Ground-Based Nuclear Explosion Monitoring Technologies, Portsmouth, 2008, pp. 824-833.
- [4] Hull, E. L.; Pehl, R. H.; Lathrop, J. R.; Martin, G. N.; Mashburn, R. B.; Miley, H. S.; Aalseth, C. E.; Hossbach, T. W.; Bower, T.W. Mechanically Cooled Large-volume Germanium Detector Systems for Nuclear Explosion Monitoring. Proceedings of the 28th Seismic Research Review: Ground Based Nuclear Explosion Monitoring Technologies, LA-UR-06-5471, 2006, pp. 822–831.
- [5] Cryogenic system design - USPAS (U.S. Particle Accelerator School) Short course Boston, MA 6/14 to 6/18/2010. https://uspas.fnal.gov/materials/10MIT/Lecture_5.1.pdf
- [6] Woodcraft, A. L. An introduction to cryogenics. <http://woodcraft.lowtemp.org>
- [7] Baudouy, B. Heat Transfer and Cooling Techniques at Low Temperature. Proceedings of the CAS-CERN Accelerator School: Superconductivity for Accelerators, Erice, Italy, 2013, pp.329-352. <https://arxiv.org/abs/1501.07153>
- [8] Donnier-Valentin, G. Cryostat design. ⁴He and ³He cryostats. Cryocourse, 2011, Grenoble. France. http://cryocourse2011.grenoble.cnrs.fr/IMG/file/Lectures/Donnier-Valentincryostat_design-v2.pdf
- [9] Parma, V. Cryostat Design. CERN Yellow Report CERN-2014-005, pp.353-399. <https://cds.cern.ch/record/1974062/files/arXiv:1501.07154.pdf>
- [10] Aalseth, C.E.; Caggiano, J. A.; Day, A. R.; Fast, J. E.; Fuller, E. S. Construction and testing of a low power cryostat for MARS. Pacific Northwest National Laboratory Document PNNL-16922. 2007.
- [11] Choi, Y. S. Natural circulation loop using liquid nitrogen for cryo-detection system. AIP Conference Proceedings, 2014, pp. 9-14. <http://dx.doi.org/10.1063/1.4860676>
- [12] Zhang, S.; Song, Y.; Lu, K.; Wang, Z.; Zhang, J.; Qin, Y. Thermal analysis of the cryostat feed through for the ITER Tokamak TF feeder. Plasma Science and Technology, 2017, 19(4).
- [13] D’Orazio, A.; Agostini, C.; Fiacco, S. Thermal Field in a NMR Cryostat. Proceedings of the COMSOL Conference, 2014. Cambridge. https://www.comsol.com/paper/download/199339/dorazio_paper.pdf

- [14] Seely, M. L.; Bonnema, E.; Cunningham, E. Heat shields: Materials and cost considerations. AIP Conference Proceedings, 2012, pp.1299-1304. <http://doi.org/10.1063/1.4707054>
- [15] Feller, J. R.; Plachta, D. W.; Mills, G.; McLean, C. Demonstration of a Cryogenic Boil-Off Reduction System Employing an Actively Cooled Thermal Radiation Shield. 16th International Cryocooler Conference, 2008. Atlanta. pp.601-609. <http://hdl.handle.net/1853/39774>
- [16] Choi, Y. S.; Kim, D. L.; Shin, D. W. Estimation of Cooldown Time in Cryocooled Superconducting Magnet System. Superconductivity and Cryogenics, 2010,12(2), 25-28.
- [17] Becker, J.A.; Cork, C. P.; Fabris, L.; Madden, N. W. Portable, low-power, mechanically cooled Ge spectrometer. Nucl Instrum Meth A, 2003, **505**(1-2), 167-169.
- [18] Siemens, “Simcenter Star-CCM+® Documentation Version 13.06”, 2018.
- [19] Shu, J-J.; Teo, J. B. M.; Chan, W. K. A New Model for Temperature Jump at a Fluid-Solid Interface. PLoS One, 2016, 11(10). <https://doi.org/10.1371/journal.pone.0165175>
- [20] Marquart, N. Introduction to the principles of vacuum physics. CAS - CERN Accelerator School : Vacuum Technology, Denmark, 1999, pp.1-24. [10.5170/CERN-1999-005.1](https://doi.org/10.5170/CERN-1999-005.1)